Quantifying the Pattern of Retinal Vascular Orientation in Diabetic Retinopathy Using Optical Coherence Tomography Angiography

Yanhui Ma (ma.1634@osu.edu)
The Ohio State University
Matthew Ohr
The Ohio State University
Cynthia Roberts
The Ohio State University

Research Article

Keywords: optical coherence tomography angiography (OCTA), diabetic retinopathy (DR)

Posted Date: January 8th, 2021

DOI: https://doi.org/10.21203/rs.3.rs-139438/v1

Version of Record: A version of this preprint was published at Scientific Reports on August 4th, 2021. See the published version at https://doi.org/10.1038/s41598-021-95219-9.

Quantifying the Pattern of Retinal Vascular Orientation in Diabetic Retinopathy Using Optical Coherence Tomography Angiography

Yanhui Ma, PhD[1*], Matthew P. Ohr, MD[1], Cynthia J. Roberts, PhD[1,2]

[1] Department of Ophthalmology and Visual Sciences, The Ohio State University, Columbus, OH
[2] Department of Biomedical Engineering, The Ohio State University, Columbus, OH

*Correspondence and requests for materials should be addressed to Y. Ma (ma.1634@osu.edu)

Abstract:

Quantitative imaging using optical coherence tomography angiography (OCTA) could provide objective tools for the detection and characterization of diabetic retinopathy (DR). In this study, we developed a novel quantitative approach using OCTA images to delineate the vessel orientation pattern of a specific region of interest, which is an orientation distribution curve depicting the probability of vessels at each angle from 0 to 360 degrees. Three quantitative metrics including vessel preferred orientation, vessel anisotropy and vessel mass were extracted from the orientation pattern and analyzed in each of eight 45° sectors at the macula. Differential retinal microvascular orientation patterns were observed between three healthy subjects and three subjects with DR. Greater variability of vessel preferred orientation ($p<0.001$) and vessel mass ($p<0.001$) was exhibited among subjects with DR than healthy in eight sectors. In the nasal-superior sector, there was a significant difference between healthy and DR subjects in preferred orientation and vessel anisotropy. The vessel mass characterized from the vascular orientation pattern was shown to be strongly correlated with the traditionally reported vessel density ($p<0.00001$). These preliminary results suggest the feasibility and advantage of our vessel orientation-based quantitative approach using OCTA to characterize DR-associated changes in retinal microvasculature.

Introduction

Diabetic retinopathy (DR) is the leading cause of vision impairment and blindness among working-age adults in the United States and worldwide [1,2], affecting more than three out of 4 individuals with diabetes mellitus of more than 15 years duration [3]. DR is classified into nonproliferative and proliferative stages. Nonproliferative diabetic retinopathy (NPDR) involves progressive intraretinal microvascular alterations that can evolve to a more advanced proliferative stage defined by extraretinal neovascularization impacting both central and peripheral vision. Earlier detection of DR is critical for preventing visual loss. Microaneurysms are usually the first visible sign of DR. However, microaneurysms do not affect vision and often go unnoticed as a result. Acellular capillaries, devoid of epithelial cells and pericytes, appear adjacent to the clusters of microaneurysms [4]. Regions of acellular capillaries in histologic sections correspond to areas of capillary non-perfusion visualized by ancillary ocular imaging [5]. Thus, imaging modalities capable of visualizing changes in retinal microvascular morphology, such as capillary dropout or non-perfusion, are mostly desired for detecting early DR pathology. Dye-based retinal angiography methods, such as fluorescein angiography (FA) and indocyanine green angiography (ICGA), are invasive, costly, time-consuming, and thus not routinely performed in patients with early-stage DR. Optical coherence tomography angiography (OCTA) has emerged as a non-invasive, three-dimensional technique for visualizing the microvasculature of the retina in different layers at micron-scale resolution [6–9].

The core principle of OCTA is the detection of OCT signal changes over time, caused by the intravascular motion of blood cells. OCTA imaging in this study was performed with Spectralis (Heidelberg Engineering, Heidelberg, Germany) OCTA Module using a full-spectrum probabilistic approach. It is worth noting that various OCTA algorithms have been established by

several manufacturers. Each OCTA system may differ with regards to the optical source, acquisition speed, scan area, retinal layer segmentation, among others. Such variances in each device may make output images different from one another, which may result in different clinical diagnostic interpretations [10–12]. Quantitative analyses of retinal capillary dropout using OCTA imaging could provide promising biomarkers of early-stage DR. Non-perfusion areas or vessel density have been used as quantitative indices to characterize DR-associated changes in retinal microvasculature, revealing that the total non-perfused area is significantly higher in DR subjects compared to normal controls [13–16], and that decreasing vessel density associates with worsening DR [17,18]. The importance of quantitative assessment of retinal microvasculature in the context of early detection of DR would lie in its distinguishing power for mild NPDR. Vessel density alone may not effectively separate mild DR from healthy subjects. Kim et al showed that no statistically significant difference of vessel density at the deep retinal layer and full layer (non-segmented) was observed between healthy and mild NPDR [17]. More quantitative imaging tools using OCTA would definitely contribute to more accurate detection of early stage DR. This study aimed to develop and apply a novel quantitative approach to capture local variations in the retinal microvascular orientation as a biomarker-level predictor of DR using OCTA imaging.

The orientation of tube-like structures has been of great interest to researchers in materials science. For instance, the orientation of individual fibers of steel-fiber reinforced cementitious composites plays an important role in the mechanical properties of the material [19,20]. Hessian matrix-based analysis offers a useful tool for quantification of tube-like structure on digital images. The matrix of the second-order partial derivative of local structure in an image is termed as the Hessian matrix. In computer vision, early approaches to ridge and valleys identification were proposed by Haralick in 1983 utilizing the second directional derivative [21]. Frangi et al applied

eigenvalue (eigenvector) analysis of the Hessian matrix to enhance the vessel structure in angiography image [22]. Specifically, the eigenvector corresponding to the smallest eigenvalue in absolute value was used to estimate the longitudinal direction of the vessel. Geometrical structure measures calculated from eigenvalues examined the likelihood of the vessel presence in the context of developing a vessel enhancement filter. This vessel filter has been widely used in angiography to improve visualization of human vasculature [23], and served as a preprocessing procedure for the segmentation of blood vessels [24].

Although the detection of vessel orientation is the intermediate step in the vessel enhancement process, a comprehensive framework for quantification of vessel orientation has never been established in retinal vasculature images. In this study, an operator combining the second derivative and Gaussian multiscale convolution is applied to tune the vesselness filter response that incorporates the eigenvalues, with the objective of enhancing the vessel structure and identifying the retinal vessel width and orientation using OCTA images. This pilot study aims to extract quantitative metrics from the pattern of retinal vascular orientation, namely, vessel preferred orientation, vessel anisotropy and vessel mass, to characterize DR-associated changes in retinal microvasculature.

Methods

Second Derivative

In computer science, the second derivative of the intensity in a gray-scale image can be used as an edge-detection operator. Zero-crossings of the second derivative for a continuous intensity profile correspond to the local maxima in the gradient of the image (first derivative) (Figure 1). For a vessel modeled as a tube with a 2-dimensional Gaussian profile with standard

deviation $s = 1$, as specified by $I_0 = \frac{1}{2\pi s^2}\exp(\frac{-x^2}{2s^2})$ (Figure 1B), the Hessian matrix can be expressed as

$$H_0 = \begin{bmatrix} \frac{\partial^2 I_0}{\partial x^2} & \frac{\partial^2 I_0}{\partial x \partial y} \\ \frac{\partial^2 I_0}{\partial x \partial y} & \frac{\partial^2 I_0}{\partial y^2} \end{bmatrix} = \begin{bmatrix} (x^2-1)I_0 & 0 \\ 0 & 0 \end{bmatrix} \quad (1)$$

Eigenvectors ($\boldsymbol{v}_1, \boldsymbol{v}_2$) and eigenvalues ($\lambda_1, \lambda_2$; $|\lambda_1| < |\lambda_2|$),) of the Hessian matrix H_0 are

$$\lambda_1 = 0; \qquad \boldsymbol{v}_1 = (0,1);$$
$$\lambda_2 = (x^2-1)I_0; \qquad \boldsymbol{v}_2 = (1,0). \quad (2)$$

The orientation of the vessel I_0 is along the y-direction, as shown in Figure 1A, and is the same as the eigenvector corresponding to the smallest eigenvalue in magnitude, i.e., $\boldsymbol{v}_1$.

For an angiography image, the intensity takes a general form $I(\boldsymbol{t})$ which can be approximated by its Taylor expansion in the neighborhood of a point $\boldsymbol{t}_0$ up to the second order to analyze the local structure,

$$I(\boldsymbol{t}) \approx I(\boldsymbol{t}_0) + \Delta\boldsymbol{t}^T \nabla I(\boldsymbol{t}_0) + \frac{1}{2}\Delta\boldsymbol{t}^T H\big(I(\boldsymbol{t}_0)\big)\Delta\boldsymbol{t} \quad (3)$$

where $\Delta\boldsymbol{t} = \boldsymbol{t} - \boldsymbol{t}_0$, $\nabla I(\boldsymbol{t}_0)$ and $H\big(I(\boldsymbol{t}_0)\big)$ are the gradient vector and Hessian matrix of the image $I(\boldsymbol{t})$ computed at the point $\boldsymbol{t}_0$. The third term in Eq.(3) gives the second-order directional derivatives,

$$\Delta\boldsymbol{t}^T H\big(I(\boldsymbol{t}_0)\big)\Delta\boldsymbol{t} = \left(\frac{\partial}{\partial \boldsymbol{t}_0}\right)\left(\frac{\partial}{\partial \boldsymbol{t}_0}\right) I(\boldsymbol{t}_0) \quad (4)$$

As it has been demonstrated with Eq. (1-2) with an ideal continuous intensity profile for vessel modeling, eigenvalue and eigenvector analysis of the Hessian matrix can reveal the vessel orientation. Eigenvector defines the direction in which it essentially just get scaled up by the linear transformation,

$$H\big(I(\boldsymbol{t}_0)\big)\,\boldsymbol{v} = \lambda \boldsymbol{v} \tag{5}$$

and it can be stated equivalently as

$$\boldsymbol{v}^T H\big(I(\boldsymbol{t}_0)\big)\,\boldsymbol{v} = \lambda \tag{6}$$

The similarity between Eq.(4) and Eq. (6) in terms of composition discloses the association of eigenvalue and the second-order structure of the image. Two orthonormal directions are mapped by the Hessian matrix onto the eigenvalues. A circle neighborhood centered at $\boldsymbol{t}_0$ is mapped by the Hessian matrix onto the second-order structure of the image. The eigenvalues extracted from the Hessian matrix describe the strength of the grey-scale variation in all directions for the pixel of interest. The eigenvector, of the smallest eigenvalue (by absolute value) corresponding to the smallest variation in those grey-scale values, delineates the orientation of the vessel in the angiography image at a specific pixel.

Multiscale Convolution

Multi-scale analysis is imperative to detect the vessels with various widths in the angiography image. When incorporating the scale σ, linear scale space theory is applied [25] to ensure the well-posed properties of the differential operator of I, such as the gradient vector and Hessian matrix. In this framework differentiation is calculated by a convolution with derivatives of Gaussians:

$$\frac{\partial}{\partial \boldsymbol{t}} I(\boldsymbol{t}, \sigma) = I(\boldsymbol{t}) * \frac{\partial}{\partial t} G(\boldsymbol{t}, \sigma) \tag{7}$$

where * denotes the convolution, and a Gaussian kernel of width σ is given by

$$G(\boldsymbol{t}, \sigma) = \frac{1}{2\pi\sigma^2} \exp\left(\frac{-||\boldsymbol{t}||^2}{2\sigma^2}\right) \tag{8}$$

where $||\boldsymbol{t}||^2$ is the squared length of vector $\boldsymbol{t}$, i.e., $x^2 + y^2$. The partial second derivative of $I(\boldsymbol{t}, \sigma)$ in the Hessian matrix can be replaced by the partial second derivative of Gaussian, for example,

$$I_{xx}(\boldsymbol{t}, \sigma) = I(\boldsymbol{t}) * \frac{\partial^2}{\partial^2 x} G(\boldsymbol{t}, \sigma) \tag{9}$$

Convolving the image with a Gaussian function can smooth out the image background noise and enhance image vessel structures. The eigenvectors and eigenvalues of the Hessian matrix depends on the scale σ of the Gaussian, and therefore are denoted as, $\boldsymbol{v}_i(\boldsymbol{t}, \sigma)$ and $\lambda_i(\boldsymbol{t}, \sigma)$, respectively (i=1,2; $|\lambda_1| < |\lambda_2|$). The condition of a line can be regarded as $\lambda_1 \approx 0$ (for an ideal line, $\lambda_1 = 0$), thus the ratio of eigenvalues has been suggested as a similarity measure of a line structure [26,27],

$$R = \frac{|\lambda_1(\boldsymbol{t}, \sigma)|}{|\lambda_2(\boldsymbol{t}, \sigma)|} \tag{10}$$

In addition to geometric measure for vessels, another important measure is defined to distinguish the vessel from the background noise, termed as a structure-ness measure [22]:

$$S = \sqrt{\lambda_1^2(\boldsymbol{t}, \sigma) + \lambda_2^2(\boldsymbol{t}, \sigma)} \tag{11}$$

S will be low for the background when there is no presence of the vessel structure as the eigenvalues will be small due to the lack of contrast. With these two measures, R and S, a filter response function is defined to detect the vessels with different widths,

$$\rho(\boldsymbol{t}, \sigma) = \exp\left(-\frac{R^2}{2\beta^2}\right)\left(1 - \exp\left(-\frac{S^2}{2\gamma^2}\right)\right) \tag{12}$$

where β and γ are suppression index. This filter is examined at different scales in the range of $\sigma_{min} \leq \sigma \leq \sigma_{max}$, which covers the range of vessel width in the angiography image. The strongest response indicates the identification of vessel width at a specific pixel,

$$\rho(\boldsymbol{t}) = \max_{\sigma_{min} \leq \sigma \leq \sigma_{max}} \rho(\boldsymbol{t}, \sigma) \tag{13}$$

The filter response will be maximum when the scale matches the width of the vessel, σ_0. The vessel orientation is estimated as $\boldsymbol{v}_1(\boldsymbol{t}, \sigma_0)$, i,e, the eigenvector corresponding to the smallest eigenvalue in magnitude $\lambda_1(\boldsymbol{t}, \sigma_0)$. Overall, this vesselness filter allows enhancing the vessel-background segmentation and detecting the vessel width and orientation simultaneously. The enhancement quality and efficiency were regulated by four filter parameters, i.e., scale range [σ_{min} σ_{max}], and suppression index, β and γ. They were empirically determined by approximating the size (in pixels) of the vessel width and evaluating the noise and background suppression.

Pattern of Retinal Vascular Orientation: preferred orientation, anisotropy and vessel mass

Localized changes in retinal microvascular orientation have not been previously quantified from OCTA images. Fig. 2 illustrates the vessel orientation extraction from a representative OCTA image. Note that the orientation of the retinal vessel can be identified at each pixel, denoted by the arrows (Fig. 2(c)). In addition to the vesselness filter, the binary filter was applied prior to the Hessian matrix-based method to extract the vessel orientation in the region of interest (ROI). Binary filter with a fixed threshold was limited by the fact that the noise level could vary among scans and even within the same scan due to deviations in the OCT reflectance signal.[28,29] In contrast, we created a binary vessel mask with a globally determined threshold using Otsu's method [30], which chooses the threshold value to minimize the intra-class variance of the black and white pixels in the image. Color maps were generated to visualize the local vessel orientation in the ROI (Fig. 3).

A polar plot of orientation distribution was generated to show the probability of vessel at each angle from 0 to 360 degrees. This orientation distribution curve exhibits the unique pattern of vasculature organization in the selected ROI. Quantitative measures of the vessel orientation

pattern can be achieved by analyzing the polar plot region encompassed by the orientation distribution curve, including preferred orientation, vessel anisotropy, and vessel mass. As shown in Fig. 4, the orientation pattern for the specific ROI (middle) depicts a roughly elliptical shape with a major axis and a minor axis. The preferred orientation is identified by the angle of the major axis. The ratio of major axis length and minor axis length is defined as the vessel anisotropy. The vessel mass is defined as the area of the shape, or the number of square pixels that covers the closed orientation distribution curve. These three quantitative metrics are independent to each other (Fig. 4).

Vessel density was calculated as the ratio of total vessel area to the total area of ROI [23] in the OCTA image. The correlation between vessel mass in the current study and traditionally reported vessel density was evaluated by Pearson correlations (6 subjects x 8 sectorial ROIs). All data analysis was conducted by using SAS software (V9.4; SAS Institute Inc., Cary, NC, USA).

Results

Subject Participants

All experiments were performed in adherence to the tenets of the Declaration of Helsinki and informed consent was obtained from all participants. This study was approved by the Institutional Review Board of The Ohio State University. OCTA scans at the macula were obtained from 3 subjects with healthy eyes and 3 subjects with DR using a commercial OCTA module (SPECTRALIS, Heidelberg Engineering). The disease severity level of the DR subjects was ranked as mild and moderate (without current evidence of macular edema).

For the Spectralis in the current study, each OCT volume scan with dimensions of 3 × 3 × 2 mm consisted of 256 clusters of B-scans, where each B-scan consisted of 256 A-scans. Active

eye-tracking (TruTrack) technology was used to correct for displacements by re-acquisition of OCT images at the correct retinal location in real-time. Any images with significant artifactual components due to blockage of OCT signal by floaters and eyelashes, residual motion artifacts, or other artifacts, were excluded from the study to avoid confounding of quantitative analysis.

Differential Retinal Microvascular Orientation Patterns between Healthy and DR Subjects

Our quantitative analysis defines the ROIs as equal-area sectors. Each 45º sector of the circular disk centered at the macular region was defined as the new ROI, namely NS, SN, ST, TS, TI, IT, IN, and NI (N=nasal, S=superior, T=temporal, I=inferior). Eight Sectorial preferred orientations of retinal microvasculature have been shown to vary within the same eye and are unaligned with their sector axis as shown in Fig. 5. Vessel orientation pattern for each sectorial ROI was quantified, such as preferred vessel orientation, vessel anisotropy and vessel mass, and compared between healthy subjects (n=3) and subjects with diabetic retinopathy (n=3).

In the TS sector, the average preferred vessel orientation of healthy subjects was similar to that of DR subjects (76.6 ± 17.1 for healthy vs 72.2 ± 18.9 for DR). The largest difference in preferred orientation between healthy and DR was observed in the NS sector (8.0 ± 1.8 for health vs 91.4 ± 44.6 for DR, $p=0.01$). Greater variability of vessel preferred orientation was exhibited among subjects with DR than healthy ($p<0.001$), particularly in the sectors of NS, IN and NI indicated by the standard deviation (44.6 vs 1.8, 50.2 vs 4.8, and 32.9 vs 5.7, respectively). The bar graph showing the distribution of preferred vessel orientation between healthy and DR subjects is given in Fig. 6(a).

Fig. 6(b) demonstrates the comparison between healthy subjects and subjects with DR, and the distribution of eight sectors in terms of the vessel anisotropy. In contrast to preferred orientation, more variability of vessel anisotropy was observed among healthy subjects, especially in the

sectors of NS, IN and NI, the same sectors that showed much greater variability of preferred vessel orientation in DR subjects. Anisotropy of sector TS in DR subjects was similar to healthy subjects (1.6 ± 0.3 for healthy vs 1.7 ± 0.4 for DR). Sector IN demonstrated the largest difference in vessel anisotropy between healthy and DR subjects (3.8 ± 1.4 for healthy vs 1.2 ± 0.1 for DR, $p=0.01$), and sector NS came next (3.3 ± 1.3 for health vs 1.5 ± 0.1 for DR, $p=0.03$).

The distribution of vessel mass in the eight sectors appeared to be relatively even in DR subjects (Fig. 6(c)), compared to vessel preferred orientation and vessel anisotropy of which the distribution displayed differences across sectors. In addition, the variability is also greater in DR subjects than healthy subjects ($p<0.001$)

Table 1 lists the quantification of retinal microvascular pattern for each individual healthy subject and DR subject in the sector of NS. Asterisk indicates statistical significance at the level of 0.05 using a t-test comparison of DR and healthy subjects. Large differences between DR and healthy subjects in the sector of NS were observed in the preferred orientation ($p=0.01$) and vessel anisotropy ($p=0.03$), despite a small sample size. No significant difference was observed in the vessel mass.

Comparison between Vessel Mass and Vessel Density

We have compared the vessel mass quantified from the vascular pattern and the vessel density calculated from the traditional method for 6 subjects and 8 sectors per subject. The vessel mass was strongly correlated with the vessel density with Pearson $R=0.95$ ($p<0.00001$). Fig. 7 provides a scatterplot of the relationship between vessel mass and vessel density.

Discussion

The accurate detection and characterization of human diabetic retinopathy are critical to define at-risk patients, anticipate progression, and assess new therapies. Vessel density over a desired region of interest is the most common quantitative assessment made with OCTA. However, localized changes in microvascular orientation have never been quantified from OCTA images, to the best of our knowledge. In this study, we developed a novel quantitative approach to delineate the pattern of retinal vascular orientation from OCTA images which generated three quantitative metrics. First, Gaussian multi-scale convolution was combined with the second derivative in an attempt to tune the vesselness filter response to the specific vessel width and orientation. Then with the identification of vessel orientation at each pixel, the pixels at a certain angle ranging from 0 to 360 degrees were integrated, which yielded the orientation pattern in the desired ROI. Preferred vessel orientation, vessel anisotropy, and vessel mass were defined to quantify the orientation pattern, reducing 360 descriptive metrics to a manageable three metrics. Our results have elucidated that this novel quantitative approach is more advanced than the traditionally reported vessel density in two aspects: 1) extra metrics were achieved by quantifying the vessel orientation pattern beyond a single quantitative analysis of vessel density. The vessel mass characterized from the vascular orientation pattern was shown to be strongly correlated with the traditionally reported vessel density. Quantification of vessel preferred orientation and anisotropy provide more additional information about the retinal vasculature. 2) Vessel preferred orientation and anisotropy may be able to effectively separate the DR from healthy subjects especially in the NS sector (Fig.6), and have the potential for the development of a biomarker for the disease.

This pilot study focused on the method development with initial, proof-of-concept results on the differential retinal microvascular orientation patterns between healthy and DR subjects to demonstrate the feasibility and advantage of this approach. The quantification in this study focused

on the full projection of the OCTA image (summing up all the retina layers in the thickness direction). Quantification of the retinal vascular pattern within different layers is currently under investigation to further analyze the regional difference and to build a database of vessel orientation pattern using OCTA with larger sample size. Another application of the retinal microvascular orientation would be to evaluate the tortuosity in vessels recognized in digital fundus images or OCTA images. Tortuosity is one of the first alterations in the retinal vasculature in hypertensive retinopathy. For instance, hypertensive patients have severe vessel tortuosity compared to healthy subjects who exhibit normal/very mild vessel tortuosity. Some approaches for tortuosity measurement have been proposed, but they do not always coincide with ophthalmologist's perception of vessel tortuosity [31]. Vessel orientation-based tortuosity evaluation warrants further investigation.

In conclusion, our novel quantitative approach using OCTA imaging allows us to map and quantify the retinal microvascular orientation pattern, which in turn holds promise for the early detection of DR-associated retinal vascular abnormalities.

Acknowledgement

This work was supported by the National Institutes of Health under Grant R01EY027399 and the Ohio Lions Eye Research Foundation under Grant W. R. Bryan Diabetic Eye Disease.

Author Contributions

Y.M. and C.J.R. conceived the original idea. C.J.R. and M.P.O. recruited the participants and acquired the OCTA imaging. Y.M. conducted the analysis. All authors wrote and reviewed the manuscript.

Competing financial interests: The authors declare no competing interests.

References

1. Congdon, N. *et al.* Causes and prevalence of visual impairment among adults in the United States. *Arch. Ophthalmol. (Chicago, Ill. 1960)* **122**, 477–485 (2004).
2. Resnikoff, S. *et al.* Global data on visual impairment in the year 2002. *Bull. World Health Organ.* **82**, 844–851 (2004).
3. Klein, R., Klein, B. E. K., Moss, S. E., Davis, M. D. & DeMets, D. L. The Wisconsin Epidemiologic Study of Diabetic Retinopathy: II. Prevalence and risk of diabetic retinopathy when age at diagnosis is less than 30 years. *Arch. Ophthalmol.* **102**, 520–526 (1984).
4. Cogan, D. G., Toussaint, D. & Kuwabara, T. Retinal vascular patterns: IV. Diabetic retinopathy. *Arch. Ophthalmol.* **66**, 366–378 (1961).
5. Kohner, E. M. & Henkind, P. Correlation of fluorescein angiogram and retinal digest in diabetic retinopathy. *Am. J. Ophthalmol.* **69**, 403–414 (1970).
6. Wang, R. K. *et al.* Three dimensional optical angiography. *Opt. Express* **15**, 4083–4097 (2007).
7. Wang, R. K., An, L., Francis, P. & Wilson, D. J. Depth-resolved imaging of capillary networks in retina and choroid using ultrahigh sensitive optical microangiography. *Opt. Lett.* **35**, 1467–1469 (2010).
8. Jia, Y. *et al.* Split-spectrum amplitude-decorrelation angiography with optical coherence tomography. *Opt. Express* **20**, 4710–4725 (2012).
9. Jia, Y. *et al.* Quantitative optical coherence tomography angiography of vascular abnormalities in the living human eye. *Proc. Natl. Acad. Sci.* **112**, E2395--E2402 (2015).
10. Li, X.-X. *et al.* A quantitative comparison of five optical coherence tomography angiography systems in clinical performance. *Int. J. Ophthalmol.* **11**, 1784 (2018).
11. Corvi, F. *et al.* Reproducibility of vessel density, fractal dimension, and foveal avascular zone using 7 different optical coherence tomography angiography devices. *Am. J. Ophthalmol.* **186**, 25–31 (2018).
12. Munk, M. R. *et al.* OCT-angiography: A qualitative and quantitative comparison of 4

OCT-A devices. *PLoS One* **12**, e0177059 (2017).

13. Hwang, T. S. *et al.* Optical coherence tomography angiography features of diabetic retinopathy. *Retina* **35**, 2371 (2015).
14. Ishibazawa, A. *et al.* Optical coherence tomography angiography in diabetic retinopathy: a prospective pilot study. *Am. J. Ophthalmol.* **160**, 35–44 (2015).
15. Salz, D. A. *et al.* Select features of diabetic retinopathy on swept-source optical coherence tomographic angiography compared with fluorescein angiography and normal eyes. *JAMA Ophthalmol.* **134**, 644–650 (2016).
16. Schottenhamml, J. *et al.* An automatic, intercapillary area based algorithm for quantifying diabetes related capillary dropout using OCT angiography. *Retina* **36**, S93 (2016).
17. Kim, A. Y. *et al.* Quantifying microvascular density and morphology in diabetic retinopathy using spectral-domain optical coherence tomography angiography. *Invest. Ophthalmol. Vis. Sci.* **57**, OCT362--OCT370 (2016).
18. Agemy, S. A. *et al.* Retinal vascular perfusion density mapping using optical coherence tomography angiography in normals and diabetic retinopathy patients. *Retina* **35**, 2353–2363 (2015).
19. Ma, Y., Zhu, H., Su, B., Hu, G. & Perks, R. The elasto-plastic behaviour of three-dimensional stochastic fibre networks with cross-linkers. *J. Mech. Phys. Solids* **110**, 155–172 (2018).
20. Herrmann, H., Pastorelli, E., Kallonen, A. & Suuronen, J.-P. Methods for fibre orientation analysis of X-ray tomography images of steel fibre reinforced concrete (SFRC). *J. Mater. Sci.* **51**, 3772–3783 (2016).
21. Haralick, R. M. Ridges and valleys on digital images. *Comput. vision, Graph. image Process.* **22**, 28–38 (1983).
22. Frangi, A. F., Niessen, W. J., Vincken, K. L. & Viergever, M. A. Multiscale vessel enhancement filtering. in *International conference on medical image computing and computer-assisted intervention* 130–137 (1998).
23. Chu, Z. *et al.* Quantitative assessment of the retinal microvasculature using optical coherence tomography angiography. *J. Biomed. Opt.* **21**, 66008 (2016).
24. Fraz, M. M. *et al.* Blood vessel segmentation methodologies in retinal images--a survey. *Comput. Methods Programs Biomed.* **108**, 407–433 (2012).

25. Florack, L. M. J., ter Haar Romeny, B. M., Koenderink, J. J. & Viergever, M. A. Scale and the differential structure of images. *Image Vis. Comput.* **10**, 376–388 (1992).
26. Sato, Y. *et al.* Three-dimensional multi-scale line filter for segmentation and visualization of curvilinear structures in medical images. *Med. Image Anal.* **2**, 143–168 (1998).
27. Lorenz, C., Carlsen, I.-C., Buzug, T. M., Fassnacht, C. & Weese, J. Multi-scale line segmentation with automatic estimation of width, contrast and tangential direction in 2D and 3D medical images. in *CVRMed-MRCAS'97* 233–242 (1997).
28. Zhang, M. *et al.* Projection-resolved optical coherence tomographic angiography. *Biomed. Opt. Express* **7**, 816–828 (2016).
29. Zhang, A., Zhang, Q. & Wang, R. K. Minimizing projection artifacts for accurate presentation of choroidal neovascularization in OCT micro-angiography. *Biomed. Opt. Express* **6**, 4130–4143 (2015).
30. Otsu, N. A threshold selection method from gray-level histograms. *IEEE Trans. Syst. Man. Cybern.* **9**, 62–66 (1979).
31. Grisan, E., Foracchia, M. & Ruggeri, A. A novel method for the automatic grading of retinal vessel tortuosity. *IEEE Trans. Med. Imaging* **27**, 310–319 (2008).

Figure Captions

Figure 1. (a) Gray-scale image of a tube-like structure with (b) an intensity profile of 2-dimensional Gaussian with standard deviation s=1. Zero-crossings of the second derivative (c) correspond to the local maxima in the first derivative (d).

Figure 2. Illustration of vessel orientation extraction from OCTA image. (a) Retinal microvasculature at the optic nerve head. (b) Two-dimensional vessel orientations were calculated by the Hessian matrix-based algorithm. (c): Blowup of (b), the arrows point the vessel directions/orientations.

Figure 3. Visualization of retinal microvascular orientation in the region of interest after vesselness filter and binary filter. Dark blue and red indicate 0 and 180 degrees for those horizontal vessels and green indicates 90 degrees for those vertical vessels.

Figure 4. Quantification of vessel orientation pattern using preferred orientation, vessel anisotropy and vessel mass. The orientation pattern (middle) for the specific ROI (left) depicts a roughly elliptical shape with a major axis and a minor axis. The preferred orientation is identified by the angle of the major axis. The ratio of major axis length and minor axis length is defined as the vessel anisotropy. The vessel mass is defined as the area of the shape. Examples of preferred orientation, vessel anisotropy, and vessel mass, are illustrated by the dashed ellipse relative to the solid ellipse (right).

Figure 5. Eight 45 º sectors were divided from a circular disk centered at the macula and each sector was defined as the region of interest. Sectorial vascular pattern with preferred vessel orientation unaligned with sector axis.

Figure 6. Difference of retinal microvascular pattern between healthy subjects (n=3) and subjects with DR (n = 3) was revealed by the distribution of (a) preferred orientation, (b) vessel anisotropy, and (c) vessel mass in eight sectors. * indicates statistically significant ($p<0.05$).

Figure 7. Scatterplot of the relationship between vessel mass and vessel density. Red dots indicate DR (3 subjects x 8 sectors) and gray dots indicate healthy (3 subjects x 8 sectors).

Table Captions

Table 1. Quantification of retinal microvascular pattern for each individual healthy subject and DR subject in the sector of NS. * indicates that significant difference between healthy and DR subjects was observed in preferred orientation and vessel anisotropy in this sector.

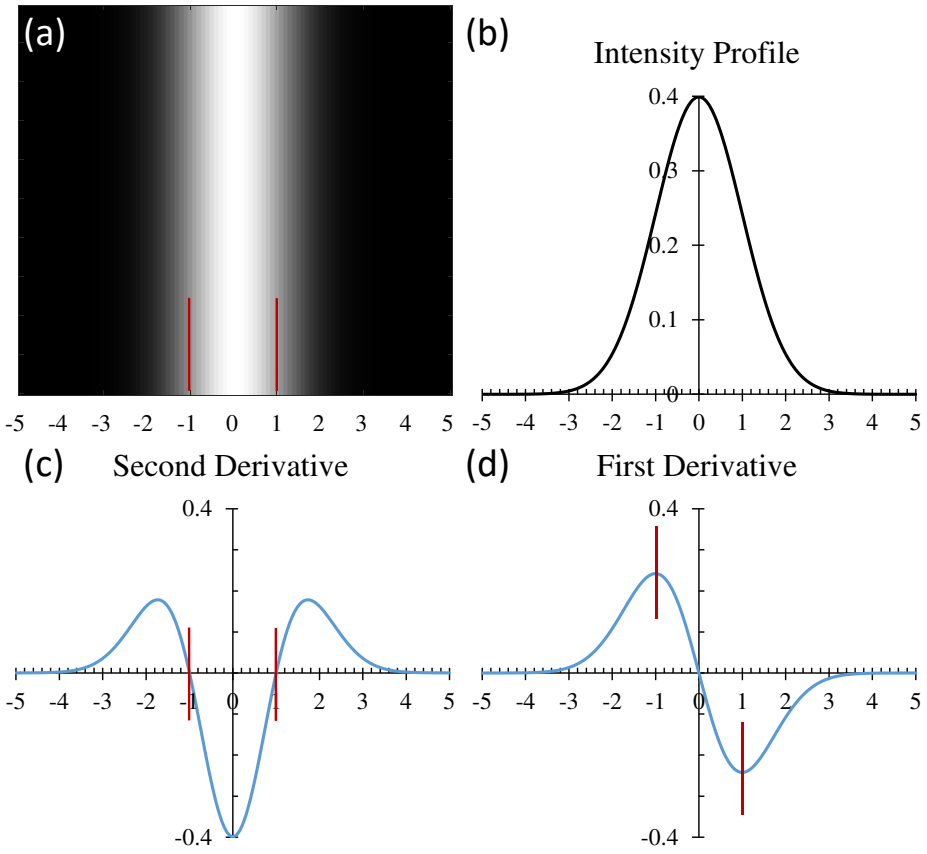

Figure 1. (a) Gray-scale image of a tube-like structure with (b) an intensity profile of 2-dimensional Gaussian with standard deviation s=1. Zero-crossings of the second derivative (c) correspond to the local maxima in the first derivative (d).

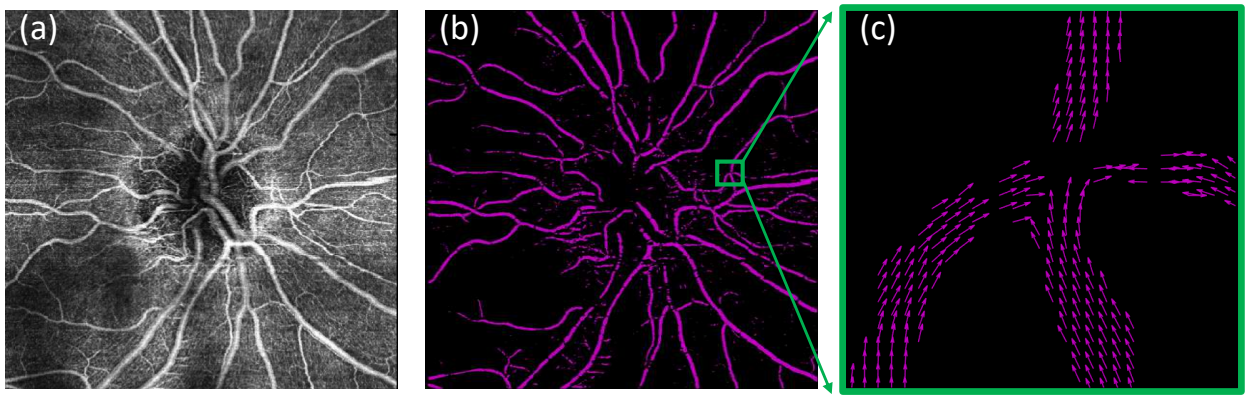

Figure 2. Illustration of vessel orientation extraction from OCTA image. (a) Retinal microvasculature at the optic nerve head. (b) Two-dimensional vessel orientations were calculated by the Hessian matrix-based algorithm. (c): Blowup of (b), the arrows point the vessel directions/orientations.

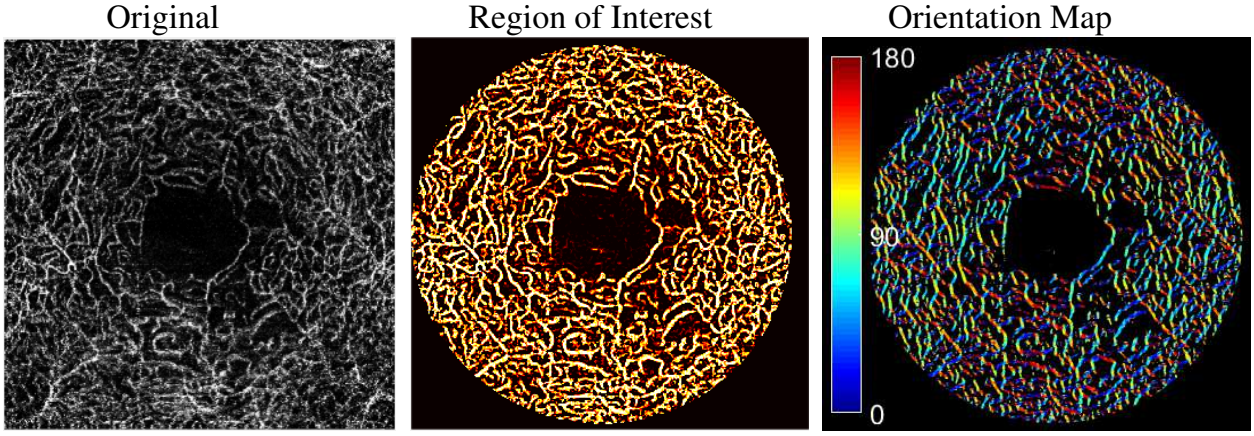

Figure 3. Visualization of retinal microvascular orientation in the region of interest after vesselness filter and binary filter. Dark blue and red indicate 0 and 180 degrees for those horizontal vessels and green indicates 90 degrees for those vertical vessels.

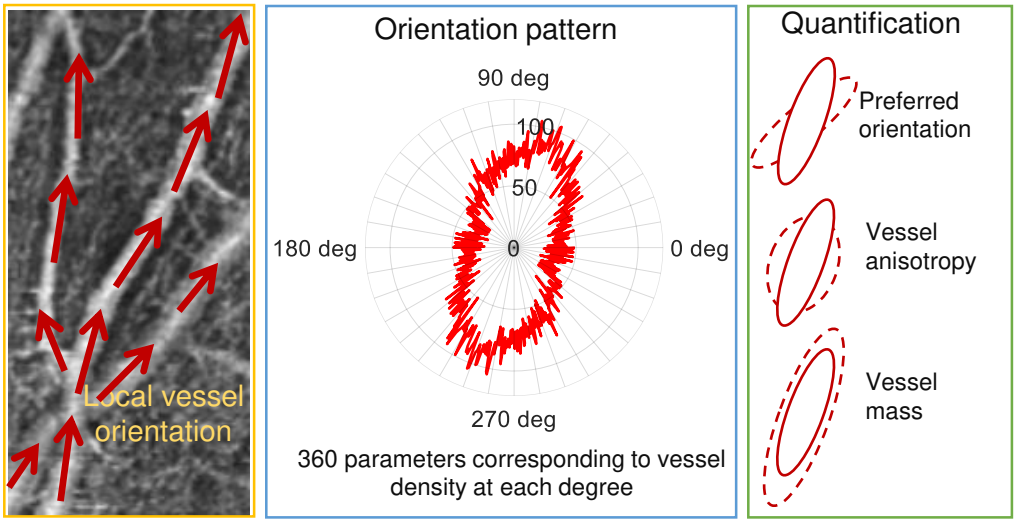

Figure 4. Quantification of vessel orientation pattern using preferred orientation, vessel anisotropy and vessel mass. The orientation pattern (middle) for the specific ROI (left) depicts a roughly elliptical shape with a major axis and a minor axis. The preferred orientation is identified by the angle of the major axis. The ratio of major axis length and minor axis length is defined as the vessel anisotropy. The vessel mass is defined as the area of the shape. Examples of preferred orientation, vessel anisotropy, and vessel mass, are illustrated by the dashed ellipse relative to the solid ellipse (right).

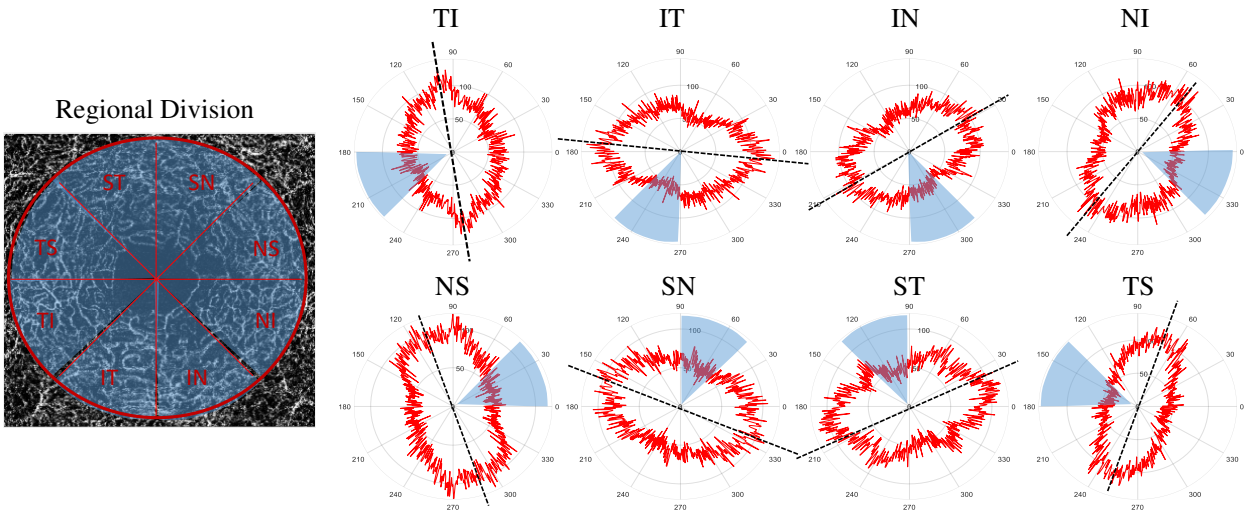

Figure 5. Eight 45 ° sectors were divided from a circular disk centered at the macula and each sector was defined as the region of interest. Sectorial vascular pattern with preferred vessel orientation unaligned with sector axis.

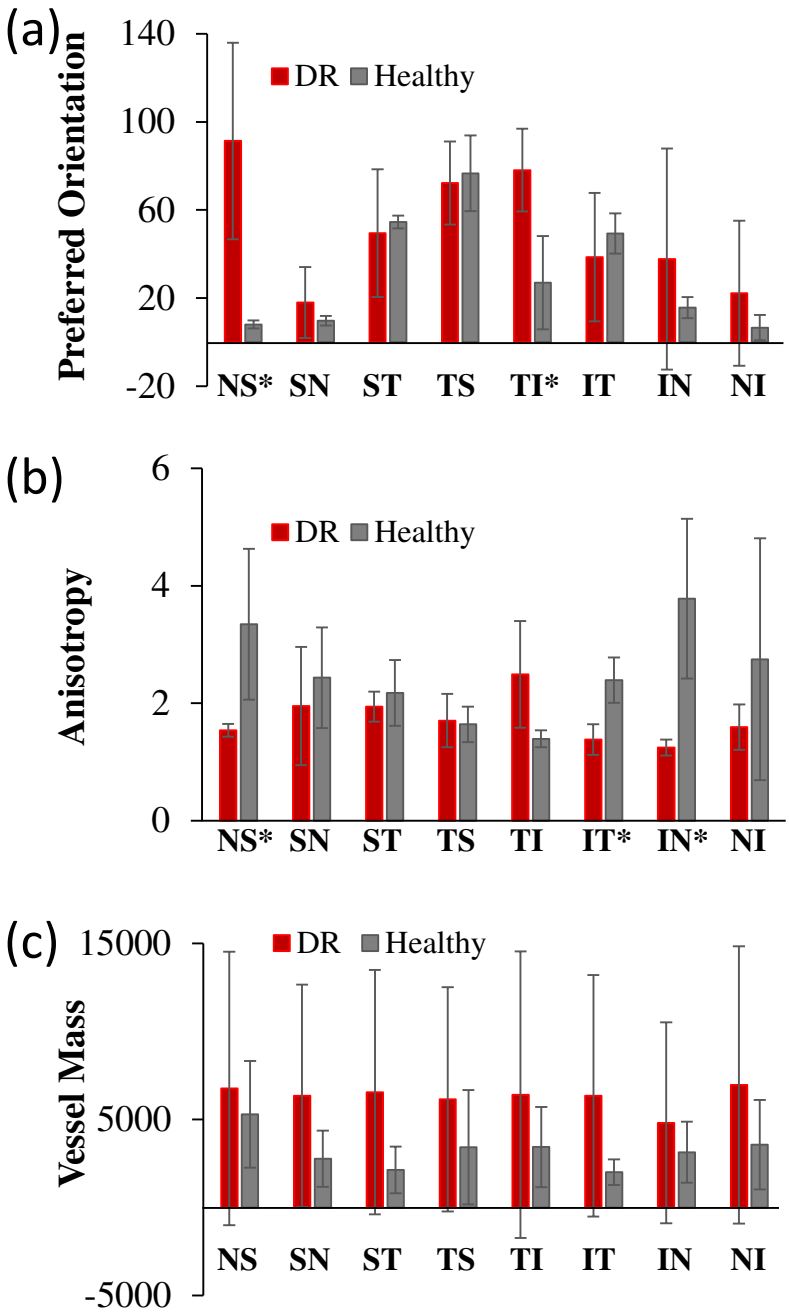

Figure 6. Difference of retinal microvascular pattern between healthy subjects (n=3) and subjects with DR (n = 3) was revealed by the distribution of (a) preferred orientation, (b) vessel anisotropy, and (c) vessel mass in eight sectors. * indicates statistically significant ($p<0.05$).

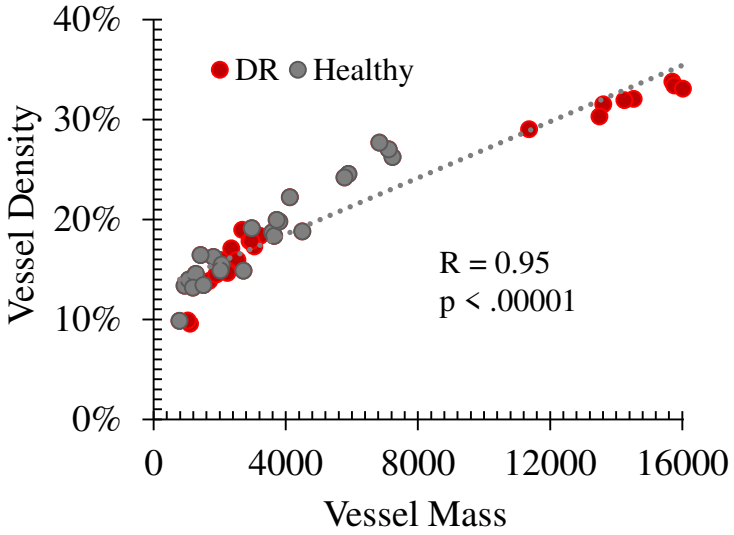

Figure 7. Scatterplot of the relationship between vessel mass and vessel density. Red dots indicate DR (3 subjects x 8 sectors) and gray dots indicate healthy (3 subjects x 8 sectors).

Table 1. Quantification of retinal microvascular pattern for each individual healthy subject and DR subject in the sector of NS. * indicates that significant difference between healthy and DR subjects was observed in preferred orientation and vessel anisotropy in this sector.

Subject	Preferred Orientation *	Vessel Anisotropy *	Vessel Mass
DR_#1	105.1	1.4	15701
DR_#2	127.5	1.6	1686
DR_#3	41.5	1.6	2899
Healthy_#1	6.2	4.8	1808
Healthy_#2	8.0	2.3	7235
Healthy_#3	9.9	3.0	6836

Figures

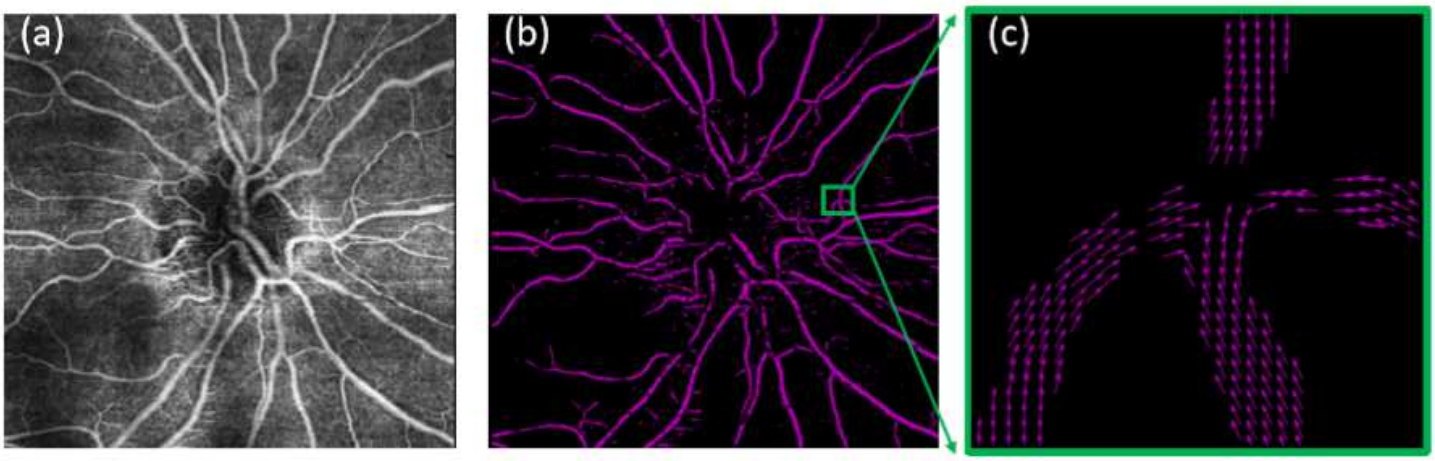

Figure 1

(a) Gray-scale image of a tube-like structure with (b) an intensity profile of 2dimensional Gaussian with standard deviation s=1. Zero-crossings of the second derivative (c) correspond to the local maxima in the first derivative (d).

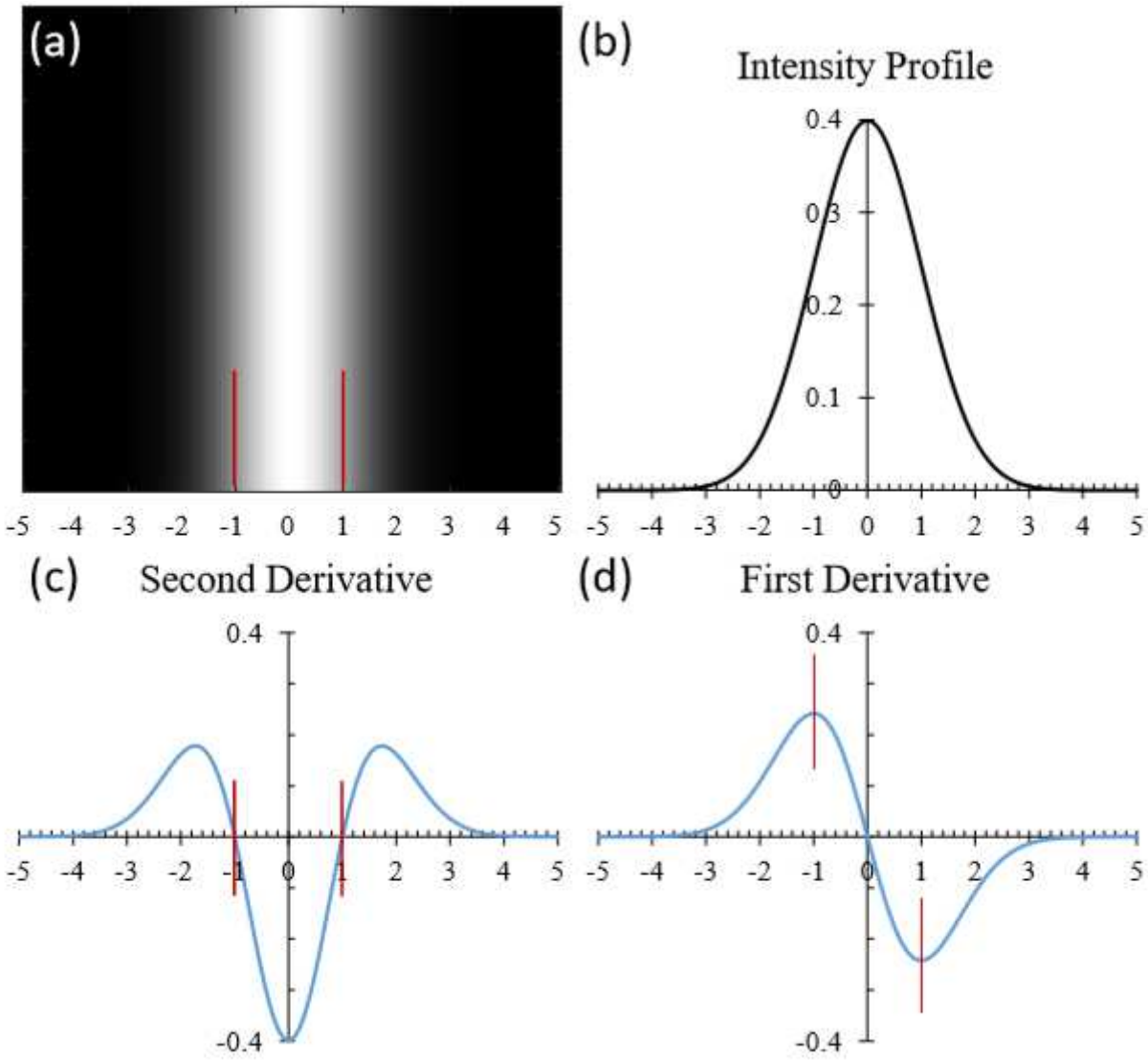

Figure 2

Illustration of vessel orientation extraction from OCTA image. (a) Retinal microvasculature at the optic nerve head. (b) Two-dimensional vessel orientations were calculated by the Hessian matrix-based algorithm. (c): Blowup of (b), the arrows point the vessel directions/orientations.

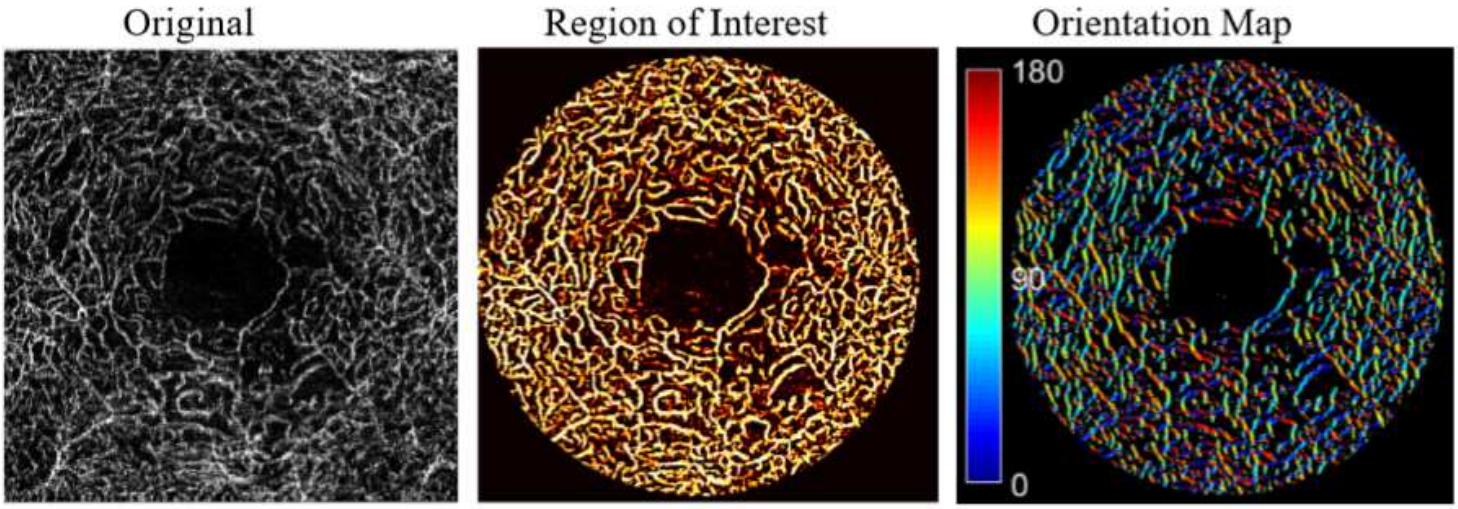

Figure 3

Visualization of retinal microvascular orientation in the region of interest after vesselness filter and binary filter. Dark blue and red indicate 0 and 180 degrees for those horizontal vessels and green indicates 90 degrees for those vertical vessels.

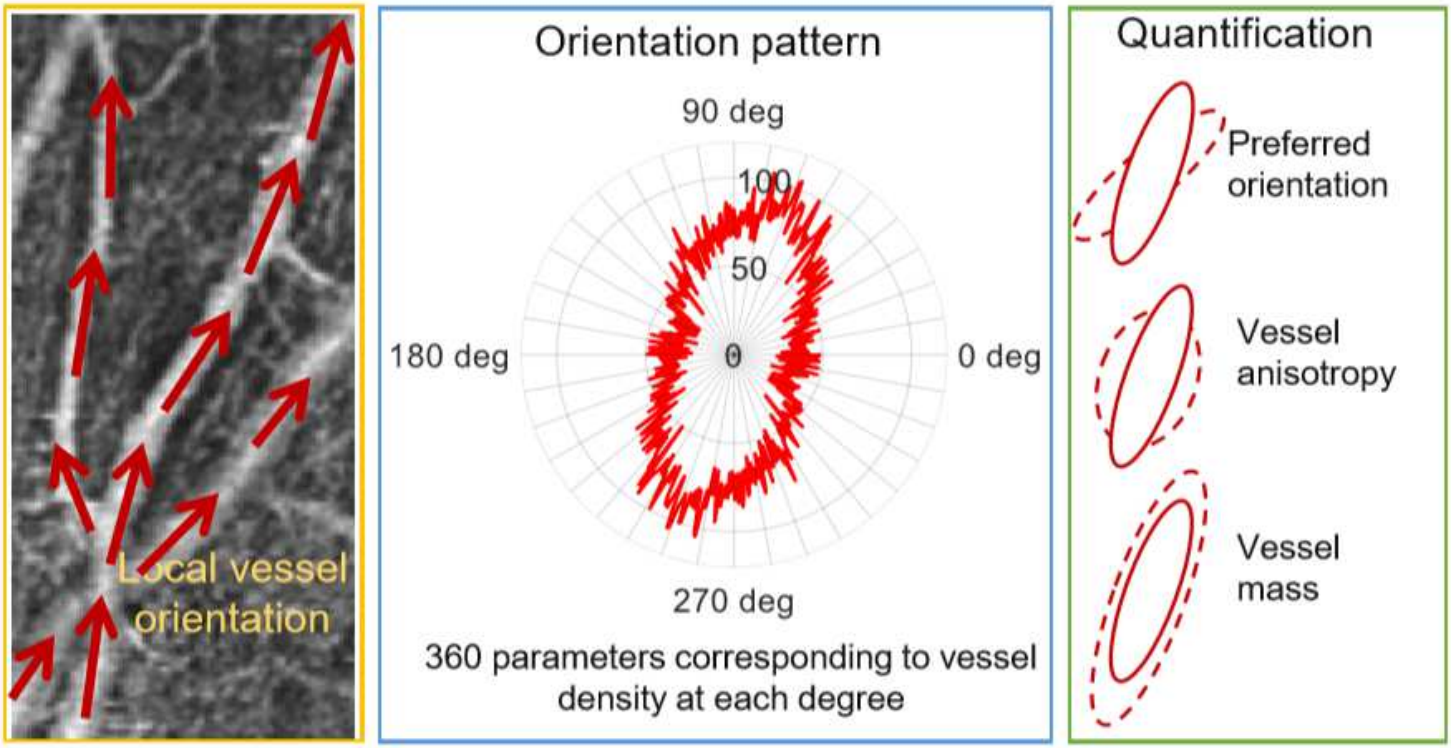

Figure 4

Quantification of vessel orientation pattern using preferred orientation, vessel anisotropy and vessel mass. The orientation pattern (middle) for the specific ROI (left) depicts a roughly elliptical shape with a major axis and a minor axis. The preferred orientation is identified by the angle of the major axis. The ratio of major axis length and minor axis length is defined as the vessel anisotropy. The vessel mass is

defined as the area of the shape. Examples of preferred orientation, vessel anisotropy, and vessel mass, are illustrated by the dashed ellipse relative to the solid ellipse (right).

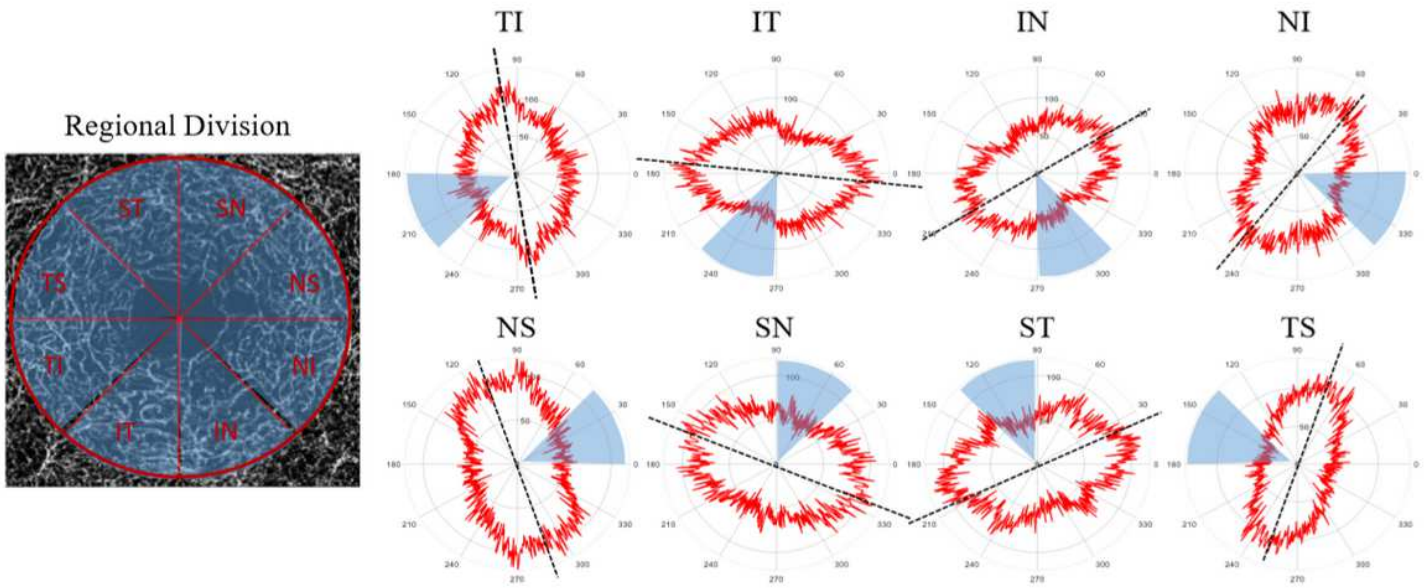

Figure 5

Eight 45 º sectors were divided from a circular disk centered at the macula and each sector was defined as the region of interest. Sectorial vascular pattern with preferred vessel orientation unaligned with sector axis.

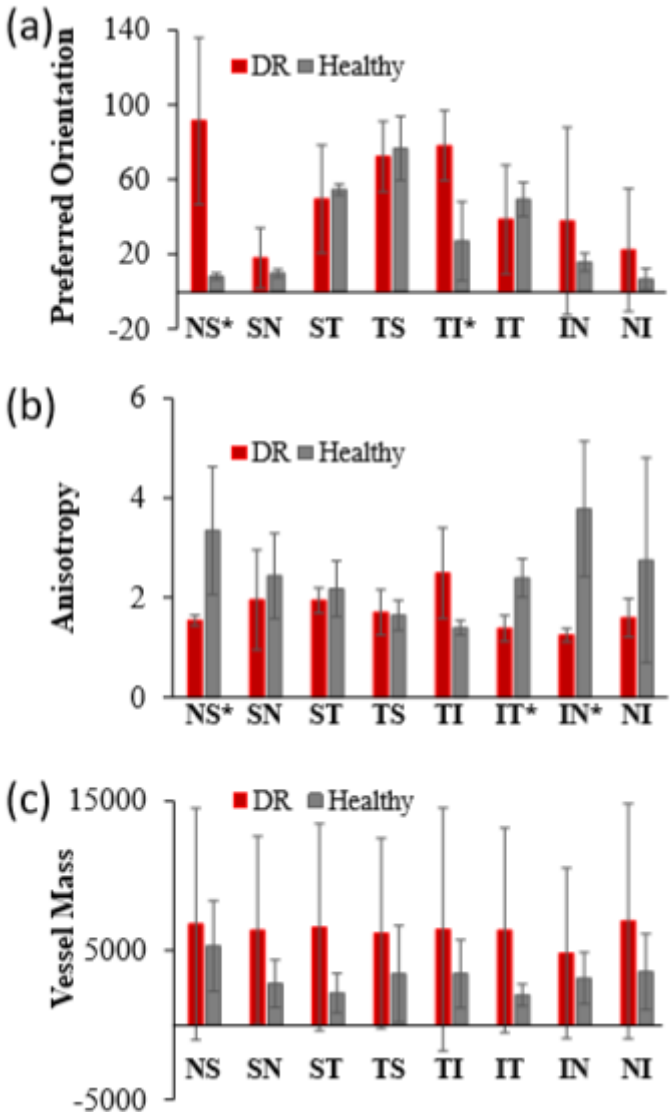

Figure 6

Difference of retinal microvascular pattern between healthy subjects (n=3) and subjects with DR (n = 3) was revealed by the distribution of (a) preferred orientation, (b) vessel anisotropy, and (c) vessel mass in eight sectors. * indicates statistically significant ($p<0.05$).

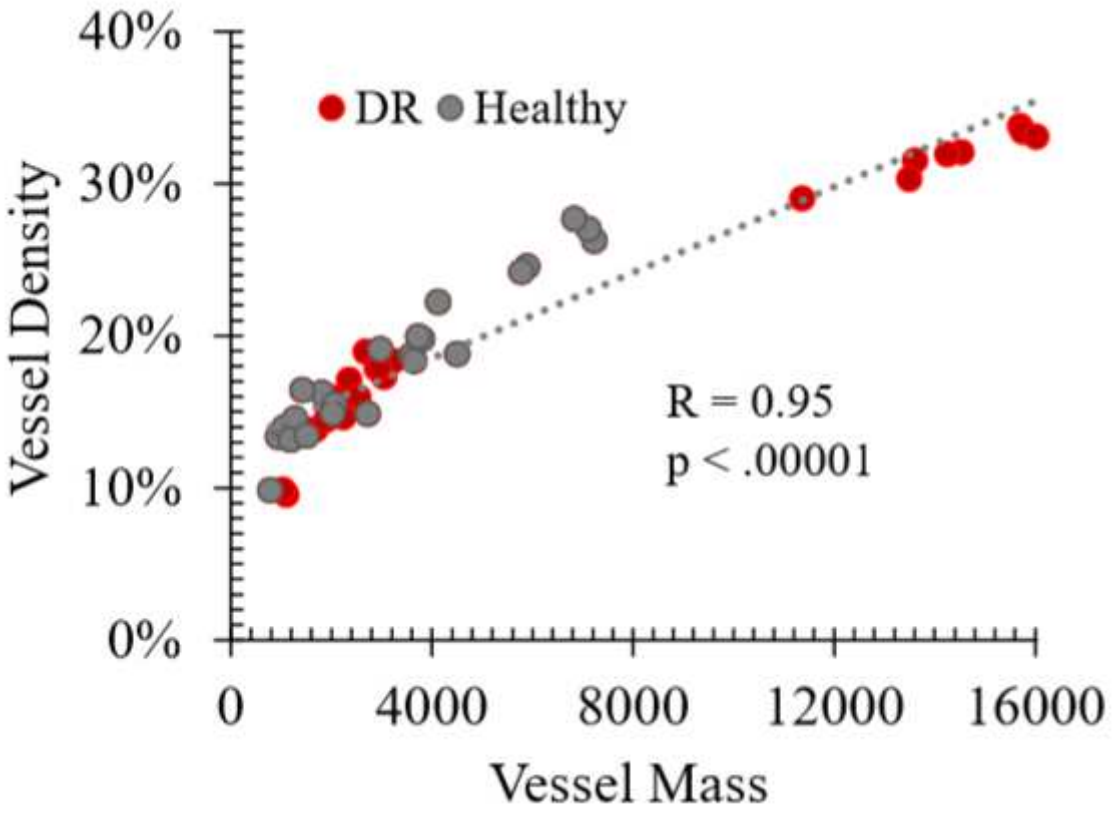

Figure 7

Scatterplot of the relationship between vessel mass and vessel density. Red dots indicate DR (3 subjects x 8 sectors) and gray dots indicate healthy (3 subjects x 8 sectors).